Journal of Computational Physics 227 (2008) 9293–9302

Contents lists available at ScienceDirect

Journal of Computational Physics

journal homepage: www.elsevier.com/locate/jcp

Short Note

Second-order accurate normals from height functions

Poorya A. Ferdowsi, Markus Bussmann *

Department of Mechanical and Industrial Engineering, University of Toronto, 5 King's College Road, Toronto, Ontario, Canada M5S 3G8

ARTICLE INFO

Article history:
Received 8 June 2007
Received in revised form 11 July 2008
Accepted 23 July 2008
Available online 7 August 2008

1. Introduction

Among Eulerian interface tracking and capturing techniques, the volume-of-fluid (VoF) method [1,8,10,11,13–17] is a popular choice, especially on structured meshes, because it can conserve volume exactly. Current VoF methods reconstruct interfaces from known volume fractions with a piecewise linear (PLIC) approximation in each interface cell, that requires an estimate of an interface normal. Such normals are also used to impose surface tension at interfaces via the CSF method [2,6], and can be used to calculate curvature.

There are various ways of calculating this normal; among others, by calculating the gradient of the discrete volume fractions; by minimizing the difference between actual volume fractions in a stencil of cells and those obtained by extending a linear interface segment into those cells; and by integrating fluid volume in one direction and then calculating the slope of these fluid "heights". Prototypical examples of these are the Parker–Youngs [11,17] normal, the LVIRA [12] method, and the ELVIRA [12] and height function (HF) [3,4,7,10] methods, respectively.

The common means of evaluating such methods is via norms based on what can be thought of as a "reconstruction error", that quantifies the area difference between an exact curve and a piecewise linear reconstruction, per unit length of the exact interface [12]:

$$\mathcal{L}^1 = \frac{1}{l}\int\int |f(x,y) - \tilde{f}(x,y)|\mathrm{d}x\,\mathrm{d}y \tag{1}$$

$f(x,y)$ and $\tilde{f}(x,y)$ are the characteristic function and the reconstructed volume fraction function, and l is the length of the exact interface. Put another way, $\mathcal{L}^1$ is the average normal distance between an exact interface and a piecewise linear reconstruction. By this measure, Parker–Youngs normals are first-order accurate, and (E) LVIRA and HF normals are second-order accurate. But it is important to note that based on this norm, any reconstruction will be at least first-order accurate, simply by virtue of the fact that the reconstruction occurs only in interface cells, which decrease in size as the mesh is refined. As a result, even when the PLIC reconstruction is based on normals that are randomly assigned rather than calculated, Eq. (1) deems this a first-order method. This norm is also limited to second-order accuracy regardless of the accuracy of an interface normal, simply because the reconstruction is done via a piecewise linear segment. To achieve higher-order accuracy in this norm, one would need to reconstruct with a higher-order technique (e.g. quadratic).

In this note we present an improved 2D HF technique that we designate HF2. Like the regular HF method, HF2 is second-order when evaluated via Eq. (1). But we also introduce a new error, that allows us to evaluate these methods in another way,

* Corresponding author.
E-mail addresses: p.ferdowsi@utoronto.ca (P.A. Ferdowsi), bussmann@mie.utoronto.ca (M. Bussmann).

0021-9991/$ - see front matter © 2008 Elsevier Inc. All rights reserved.
doi:10.1016/j.jcp.2008.07.014

by comparing the calculated normal to an "exact" one, that we define as the average normal evaluated along an exact interface segment. In this way, we can then describe any method via two norms: the first based on the position of the interface (Eq. (1)), and the second based on the accuracy of the normal. By these measures, as we will show, the Parker–Youngs method is first-order accurate when evaluating position and zero-order when evaluating the normal; the (E)LVIRA and HF methods are second-order for position and first-order for normals; and only the HF2 method is second-order accurate based on both norms.

2. Height functions (HF) revisited

In a two-dimensional PLIC method, each interface is reconstructed with a line segment indicated by a normal, $\vec{n} = (n_x, n_y)$ and a constant k:

$$n_x x + n_y y = k \tag{2}$$

We confine ourselves to a study of $y - h(x) = 0$. When $y = h(x)$ is continuous and differentiable on an arbitrary interval $[x_L, x_R]$, a normal $\vec{n}$ at any point inside the interval is:

$$\vec{n} = -h'(x)\hat{i} + \hat{j} \tag{3}$$

and $h'(x)$ is the first derivative of the function $h(x)$. Eq. (3) suggests that a good estimate of $h'(x)$ will lead to a reasonable approximation for the normal vector $\vec{n}$.

According to the mean value theorem illustrated in Fig. 1, for any interval $[x_L, x_R]$, we can find a line which is tangent to the curve $h(x)$ with a slope of:

$$m = -\frac{n_x}{n_y} = h'(x_c) = \frac{h(x_R) - h(x_L)}{x_R - x_L} \tag{4}$$

where $x_c \in [x_L, x_R]$; note that x_c is not necessarily the midpoint of the interval.

Now consider a discretized domain. One can obtain a normal, $\vec{n}_{\text{num}}$, for the cell (i,j) based on the mean value theorem using the 3×7 stencil shown in Fig. 2:

$$\vec{n}_{\text{num}} = (h(x_{i-1}) - h(x_{i+1}))\vec{i} + (x_{i+1} - x_{i-1})\vec{j} \tag{5}$$

where:

$$h(x_{i'}) = \sum_{j'=j-3}^{j+3} f_{i'j'} A_{i'j'} \quad \text{for } i' = i-1, i, \;\; i+1 \tag{6}$$

$A_{i,j}$ and $f_{i,j}$ are the area and the volume fraction of cell (i,j). This is the so-called height function (HF) technique [3,4,7,10].

3. A new error norm

Before we proceed to improve the HF method, we now define a new error norm by introducing an average normal $\vec{n}_{\text{ave}}$ that is calculated by evaluating the average value of $h'(x)$ along a curve segment:

$$\vec{n}_{\text{ave}} = -h'_{\text{ave}}\vec{i} + \vec{j} \tag{7a}$$

$$h'_{\text{ave}} = \frac{\int_{x=x_L}^{x=x_R} h'(x)\,\mathrm{d}l}{\int_{x=x_L}^{x=x_R} \mathrm{d}l} \tag{7b}$$

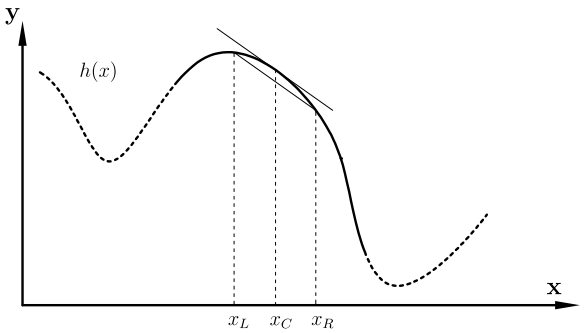

Fig. 1. Graphical representation of the mean value theorem. $x_c \in [x_L, x_R]$, although x_c is not necessarily the center point of the interval.

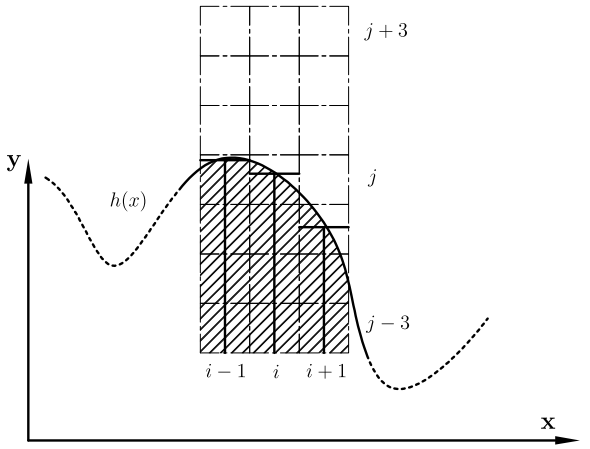

(a) $h(x)$ crosses one cell in column i

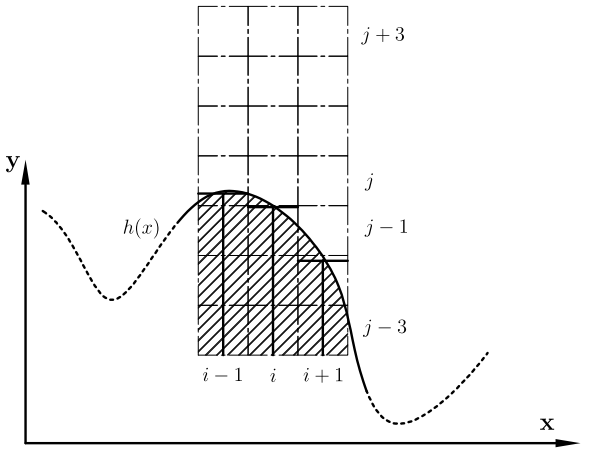

(b) $h(x)$ crosses two cells in column i

Fig. 2. Height functions in two configurations. In (b), the original HF method yields the same normal for cells (i,j) and $(i,j-1)$, while the HF2 method treats the interfaces in each of these cells separately.

where $\mathrm{d}l = \sqrt{1 + (h'(x))^2}\,\mathrm{d}x$. Unfortunately, for some functions, an analytical calculation of the integrals in Eq. (7b) is impossible. In such cases, one can use a numerical integration (e.g. trapezoidal) technique. It is trivial to show that this definition of an average normal yields an exact value for a line, and for a circle, $\vec{n}_{\text{ave}}$ is the normal at the midpoint of an arc segment. For other curves, it should be noted that $\vec{n}_{\text{ave}}$ is not a pointwise quantity, but rather an average calculated along a curve segment.

To evaluate a normal for the purpose of reconstruction, we are interested only in the orientation of the normal, and not its magnitude, and so we calculate the angle between $\vec{n}_{\text{ave}}$, that we consider a good estimate of an "exact" normal, and $\vec{n}_{\text{num}}$. Thus, we define the following norms:

$$\begin{aligned} L_1 &= \tfrac{1}{l}\sum l_i \cos^{-1}(\hat{n}_{\text{ave}} \cdot \hat{n}_{\text{num}}) \\ L_2 &= \tfrac{1}{l}\sqrt{\sum (l_i \cos^{-1}(\hat{n}_{\text{ave}} \cdot \hat{n}_{\text{num}}))^2} \\ L_\infty &= \max(\cos^{-1}(\hat{n}_{\text{ave}} \cdot \hat{n}_{\text{num}})) \end{aligned} \tag{8}$$

where l and l_i are the total length of the exact interface and the length of a segment of the exact interface in a cell, and the sums are over all interface cells in a domain. Note that $\hat{n}_{\text{ave}}$ and $\hat{n}_{\text{num}}$ are the unit normals in the direction of $\vec{n}_{\text{ave}}$ and $\vec{n}_{\text{num}}$, respectively.

4. Second-order accurate normals from height functions (HF2)

Returning to HFs, it is clear that $\hat{n}_{\text{num}}$ approaches $\hat{n}_{\text{ave}}$ with mesh refinement, because $h'(x_c) \to h'_{\text{ave}}$ when $x_L \to x_R$. That is, the integrals in Eq. (7b) become an evaluation of $h'(x)$ at the point x_c. Since a central difference scheme is used in this method, then according to Eq. (5), one would naively expect that HFs are second-order accurate based on the new norm. Yet as we

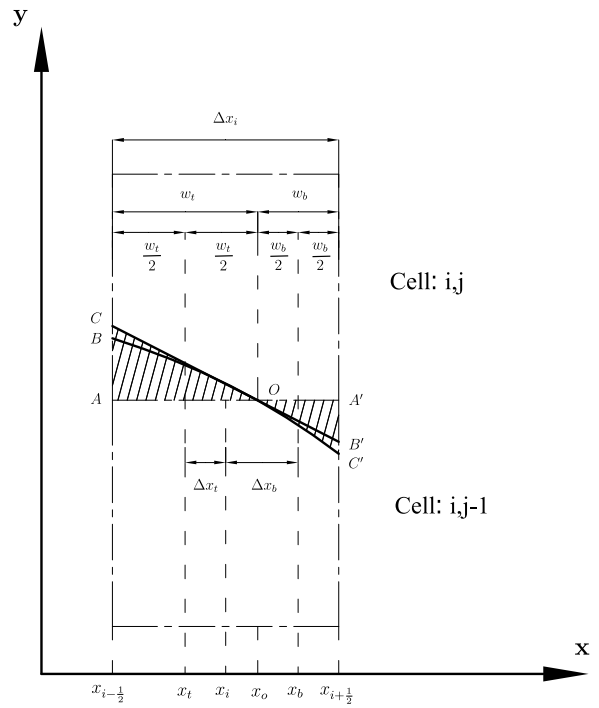

Fig. 3. Parameters for the HF2 technique. $C'OB$ is the exact interface and CB' is the line tangent to the interface at the intersection point O.

will show, this method is only first-order accurate on fine grids. Why? As shown in Fig. 2(a), when an interface in the central column crosses just one cell, Eq. (5) yields a reasonable value for an average normal in the central cell (i,j). However, when an interface crosses two cells in the central column (e.g. see Fig. 2(b)), the traditional height function technique assigns the same normal to both cells (i,j) and $(i,j-1)$, and this value deviates significantly from the exact normal in either cell. Now we introduce the HF2 technique, that ameliorates this shortcoming at little expense.

Consider Figs. 2(b) and 3: we are looking for the most accurate normal in a cell (i,j), which is reasonably close to the mid-point of the interface in the interval $x_{i-\frac{1}{2}} < x < x_o$, where x_o is the x component of the point at which the interface intersects the lower face of the cell (i,j). The ordinary HF technique yields a normal near the mid-point of the interface between $x = x_{i-\frac{1}{2}}$ and $x = x_{i+\frac{1}{2}}$. The HF2 method modifies the ordinary HF technique to obtain a normal near the mid-point of the interface confined by the two faces at $x = x_{i-\frac{1}{2}}$ and $y = y_{j-\frac{1}{2}}$, as illustrated in Fig. 3.

In what follows, we derive a methodology for the configuration of Fig. 3. We begin by using the Taylor series to obtain improved slopes at x_t and x_b:

$$m_t = m_i - \Delta x_t \frac{\mathrm{d}m_i}{\mathrm{d}x} + \mathrm{O}(\Delta x_t^2) \tag{9a}$$

$$m_b = m_i + \Delta x_b \frac{\mathrm{d}m_i}{\mathrm{d}x} + \mathrm{O}(\Delta x_b^2) \tag{9b}$$

$$m_i = \frac{h_{i+1} - h_{i-1}}{x_{i+1} - x_{i-1}} \tag{9c}$$

The subscripts 't' and 'b' refer to the *top* and *bottom* interface segments, with respect to the direction of n_y. Eqs. (9) yield slopes for the top and bottom interfaces that are greater and smaller than the slope obtained from the HF technique. In other words, as one might expect, the HF slope is bounded by the two slopes of the HF2 technique.

Now we focus on the term dm_i/dx in Eq. (9). For a non-uniform grid, by means of a Taylor series expansion around x_i one can obtain the second derivative of the function h by elimination of its first derivative:

$$\frac{\mathrm{d}m_i}{\mathrm{d}x} = \frac{\mathrm{d}^2 h}{\mathrm{d}x^2} = \frac{1}{\Delta x_i}\left(\frac{1}{\Delta x_{i+\frac{1}{2}}} h_{i+1} - \left(\frac{1}{\Delta x_{i+\frac{1}{2}}} + \frac{1}{\Delta x_{i-\frac{1}{2}}}\right) h_i + \frac{1}{\Delta x_{i-\frac{1}{2}}} h_{i-1}\right) \tag{10}$$

where $\Delta x_{i+\frac{1}{2}} = x_{i+1} - x_i$, $\Delta x_{i-\frac{1}{2}} = x_i - x_{i-1}$ and $\Delta x_i = \frac{1}{2}(\Delta x_{i+\frac{1}{2}} + \Delta x_{i-\frac{1}{2}})$. It is evident that $\mathrm{d}m_i/\mathrm{d}x$ is zero for a linear interface. That is, HF2 and HF are the same and exact when an interface is linear. For Eqs. (9) and (10) everything is known except Δx_t and Δx_b; these values can be obtained from geometrical considerations. As shown in Fig. 3, the interface can be approximated by a line tangent to the interface at point x_o, although as we only know the volume fractions, the exact location of x_o is unknown.

But consider that triangles OAC and $OA'B'$ are similar, and that with mesh refinement, the areas OBC and $OB'C'$ go to zero; then:

$$OAB \to OAC$$
$$OA'B' \to OA'C'$$

With these assumptions, we approximate:

$$\frac{w_t}{w_b} = \sqrt{\frac{A(OAC)}{A(OA'B')}} \approx \sqrt{\frac{f_{i,j}A_{i,j}}{(1-f_{i,j-1})A_{i,j-1}}} = \beta \tag{11}$$

where $w_b = x_{i+\frac{1}{2}} - x_o$, $w_t = x_o - x_{i-\frac{1}{2}}$, and A denotes area. Therefore:

$$w_t = \frac{\beta}{\beta+1}\Delta x_i \tag{12a}$$
$$w_b = \frac{1}{\beta+1}\Delta x_i \tag{12b}$$

From Fig. 3 it is clear that:

$$\Delta x_t = \frac{w_t}{2} + w_b - \frac{\Delta x_i}{2} \tag{13a}$$
$$\Delta x_b = \frac{w_b}{2} + w_t - \frac{\Delta x_i}{2} \tag{13b}$$

Now we obtain Δx_t and Δx_b based on the volume fractions and the cell widths by substituting Eqs. (12) into Eqs. (13):

$$\Delta x_t = \frac{1}{2(\beta+1)}\Delta x_i \tag{14a}$$
$$\Delta x_b = \frac{\beta}{2(\beta+1)}\Delta x_i \tag{14b}$$

This completes the derivation of normals for the configuration of Fig. 3.

More generally, for either horizontal or vertical stencils, the methodology can be summarized as follows. We first estimate the sign of the normal components with a 3×3 stencil:

$$\begin{aligned}\alpha_x &= \operatorname{sgn}\left(\sum_{j'=j-1}^{j+1}(f_{i+1,j'} - f_{i-1,j'})\right)\\ \alpha_y &= \operatorname{sgn}\left(\sum_{i'=i-1}^{i+1}(f_{i',j+1} - f_{i',j-1})\right)\end{aligned} \tag{15}$$

where sgn() is the sign function. The normal to the interface (n_x, n_y) can then be calculated as follows:

$$\begin{aligned}n_x^{i,j} &= \begin{cases}\alpha_x\left|h_{i+1} - h_{i-1} - \frac{\alpha_x\alpha_y\beta}{1+\beta}\ddot{h}_i\right| & \text{if } 0 < f_{i,j},\ f_{i,j-1} < 1\\ \alpha_x\left|h_{i+1} - h_{i-1} + \frac{\alpha_x\alpha_y}{1+\beta}\ddot{h}_i\right| & \text{if } 0 < f_{i,j},\ f_{i,j+1} < 1\end{cases}\\ \ddot{h}_i &= \frac{\Delta x_i}{\Delta x_{i+\frac{1}{2}}}h_{i+1} - \left(\frac{\Delta x_i}{\Delta x_{i+\frac{1}{2}}} + \frac{\Delta x_i}{\Delta x_{i-\frac{1}{2}}}\right)h_i + \frac{\Delta x_i}{\Delta x_{i-\frac{1}{2}}}h_{i-1}\\ n_y^{i,j} &= 2\alpha_y\Delta x_i\\ \beta &= \begin{cases}\sqrt{\left|\frac{\frac{1}{2}(1-\alpha_y)-f_{i,j}}{\frac{1}{2}(1+\alpha_y)-f_{i,j-1}}\right|\frac{A_{i,j}}{A_{i,j-1}}} & \text{if } 0 < f_{i,j},\ f_{i,j-1} < 1\\ \sqrt{\left|\frac{\frac{1}{2}(1-\alpha_y)-f_{i,j+1}}{\frac{1}{2}(1+\alpha_y)-f_{i,j}}\right|\frac{A_{i,j+1}}{A_{i,j}}} & \text{if } 0 < f_{i,j},\ f_{i,j+1} < 1\end{cases}\end{aligned} \tag{16}$$

Note that when β approaches zero or infinity (as happens when an interface crosses three adjacent cells), the HF2 normal approaches that of the HF normal.

5. Results

In this section we evaluate normals obtained by the ELVIRA (EL), Parker–Youngs (PY), height function (HF), and improved height function (HF2) methods. We reconstruct a circle (constant curvature and monotonic variation of normal direction), a cosine hyperbolic function (monotonic smooth variation of curvature and normal direction), a cosine wave (periodic variation of curvature and normal direction) and a Gaussian wave (abrupt variation of curvature and normal direction) in a 2D square domain of unit length. The four curves are:

Table 1
Old and new error norms for a circle of unit radius on a uniform square grid

Cells	L_1	L_2	L_∞	$\mathcal{L}_1$
(a) PY				
2	3.667E−02	3.250E−02	5.500E−02	6.241E−03
4	7.165E−03	3.855E−03	9.614E−03	1.658E−03
8	1.106E−02	5.408E−03	8.561E−02	6.303E−04
16	1.365E−02	4.427E−03	6.358E−02	2.206E−04
32	1.531E−02	3.363E−03	7.022E−02	1.207E−04
64	1.538E−02	2.400E−03	6.288E−02	5.744E−05
128	1.568E−02	1.685E−03	6.028E−02	2.766E−05
256	1.578E−02	1.190E−03	6.103E−02	1.357E−05
(b) EL				
2	5.280E−02	4.129E−02	6.811E−02	6.326E−03
4	2.419E−02	1.381E−02	5.356E−02	2.191E−03
8	7.020E−03	2.767E−03	5.559E−02	5.346E−04
16	7.741E−03	2.400E−03	2.493E−02	1.595E−04
32	2.206E−03	5.657E−04	1.494E−02	3.713E−05
64	1.435E−03	2.604E−04	9.708E−03	9.757E−06
128	6.450E−04	8.684E−05	5.884E−03	2.465E−06
256	3.287E−04	3.119E−05	3.354E−03	6.143E−07
(c) HF				
2	1.497E−01	1.368E−01	3.129E−01	6.326E−03
4	4.311E−02	3.024E−02	1.318E−01	3.158E−03
8	1.126E−02	5.061E−03	7.846E−02	5.842E−04
16	7.614E−03	2.304E−03	2.864E−02	1.557E−04
32	2.506E−03	5.702E−04	1.861E−02	3.695E−05
64	1.394E−03	2.290E−04	9.274E−03	9.383E−06
128	6.330E−04	7.260E−05	5.493E−03	2.347E−06
256	3.274E−04	2.673E−05	2.708E−03	5.904E−07
(d) HF2				
2	1.131E−01	9.394E−02	2.032E−01	7.646E−03
4	2.755E−02	1.569E−02	7.203E−02	2.308E−03
8	5.131E−03	2.363E−03	1.624E−02	5.228E−04
16	1.172E−03	3.499E−04	4.045E−03	1.061E−04
32	2.940E−04	6.933E−05	9.698E−04	3.094E−05
64	7.256E−05	1.131E−05	2.278E−04	7.404E−06
128	1.824E−05	2.204E−06	6.120E−05	1.931E−06
256	4.559E−06	3.847E−07	1.513E−05	4.769E−07

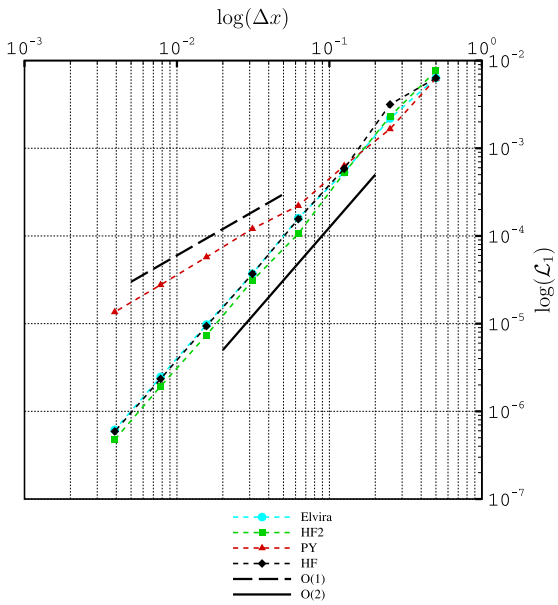

Fig. 4. Comparison of the $\mathcal{L}_1$ error norm for normals obtained by various methods for a circle. O(1) and O(2) show orders of accuracy equal to 1 and 2, respectively.

$$\text{Circle}: \quad y = \sqrt{1 - x^2} \tag{17a}$$

$$\text{Cosine hyperbolic}: \quad y = \cosh(x + 1) - 2 \tag{17b}$$

$$\text{Cosine wave}: \quad y = \frac{1 - \cos(\pi x)}{2} \tag{17c}$$

$$\text{Gaussian wave}: \quad y = \frac{1}{10} + \frac{3}{4}\exp[-25(x - 1)^2] \tag{17d}$$

For the circle, we evaluate both $\mathcal{L}^1$ and norms based on the new error, while for the others we evaluate the order of accuracy of methods only via the new norms.

Regarding the implementation, note that we extended the domain by three ghost cells to accurately evaluate the various methods to the domain boundaries. The constant of the linear interface was calculated based on the direct method presented in [5,15]. The volume fractions were obtained to machine precision by a recursive mesh refinement method. Finally, when the variation of volume fractions in any column of the stencil was not monotonic, we used the strategies in [9] to improve the results for both the HF and HF2 methods.

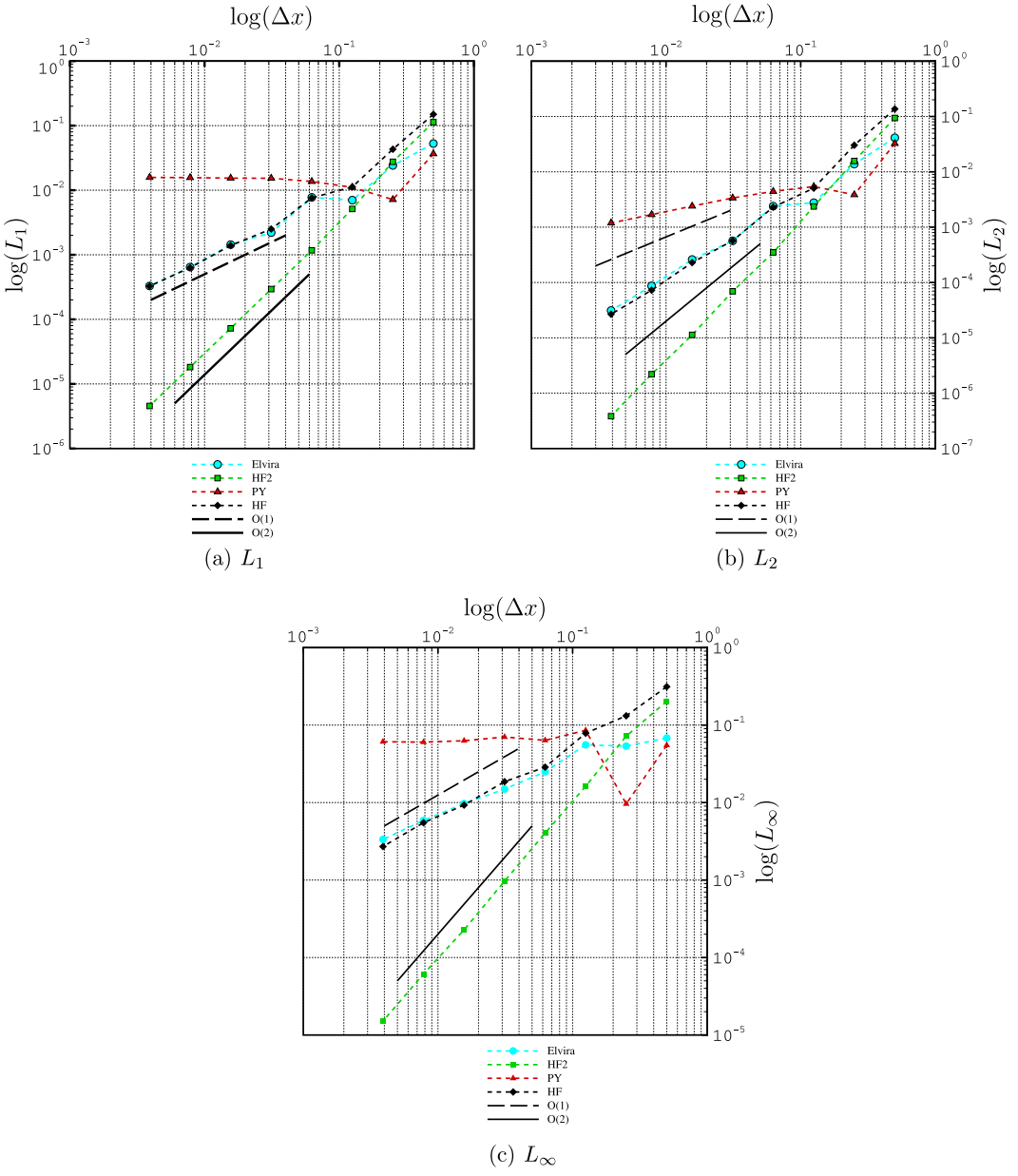

Fig. 5. Comparison of L error norms for normals obtained by various methods for a circle.

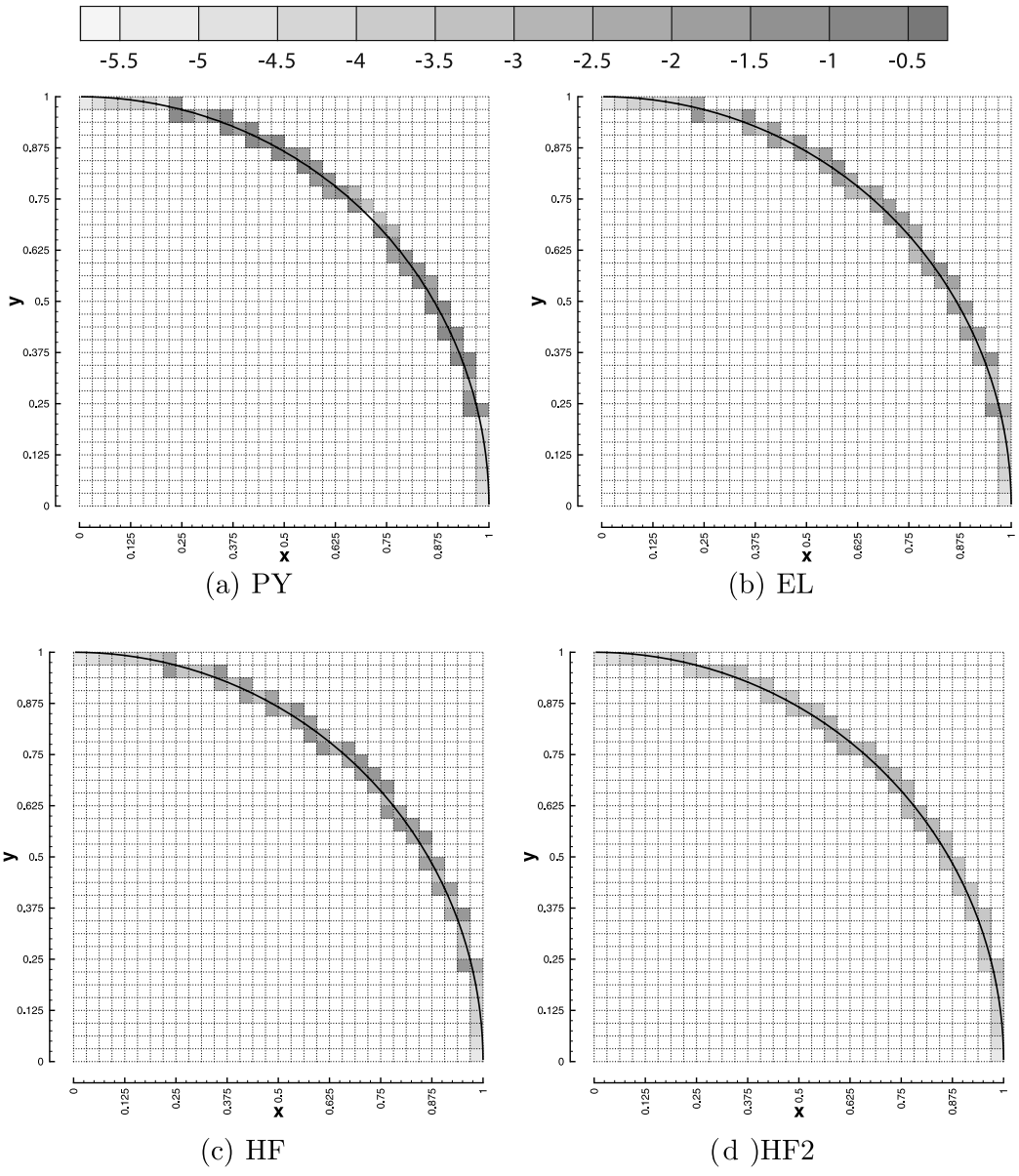

Fig. 6. Distribution of error $(\log(\cos^{-1}(\hat{n}_{\text{ave}} \cdot \hat{n}_{\text{num}})))$ and reconstructed interfaces for a circle on 32×32 grid, with normals obtained by various methods.

We now turn to the results. All error norms are shown in Table 1(a)–(d), for a circle resolved by various uniform grids. Fig. 4 illustrates $\mathcal{L}^1$: we see that the PY method is first-order, while the others are second-order accurate. As was explained previously, it is not possible to evaluate an accuracy more than two via this norm definition when the reconstruction is piecewise linear. At best, based on this norm, it appears that HF2 normals are only slightly more accurate than the others.

L_1, L_2, and L_∞ norms are shown in Fig. 5(a)–(c), and clearly show that for well-resolved circles, HF2 is the only second order accurate method, based on the new norms. The distribution of normals error on the circle, and the reconstructed interfaces obtained from all methods, are portrayed in Fig. 6. The error distributions show that when an interface crosses three cells in a row, then the HF2 and HF normals are identical and more accurate than the others. But when an interface is skewed and only crosses two cells of the height function stencil, then HF2 is much more accurate than HF. Fig. 6 also shows that the HF2 error is a minimum when the interface is aligned with the mesh, and increases gradually to a maximum when the interface direction is diagonal to the mesh. Conversely, when using HF, ELVIRA, and PY, the maximum error occurs at various locations or along a few directions. Error distributions of other curves are similar to those of the circle when a curve is well-resolved; when interface curvature is large the maximum HF2 error occurs at or near the cell with the largest curvature.

Fig. 5(a)–(c) also clearly indicate that at very low resolutions the PY normals are as accurate as those of any of the methods, and that only with refinement do the other methods outperform. This is noteworthy because in practice VoF methods

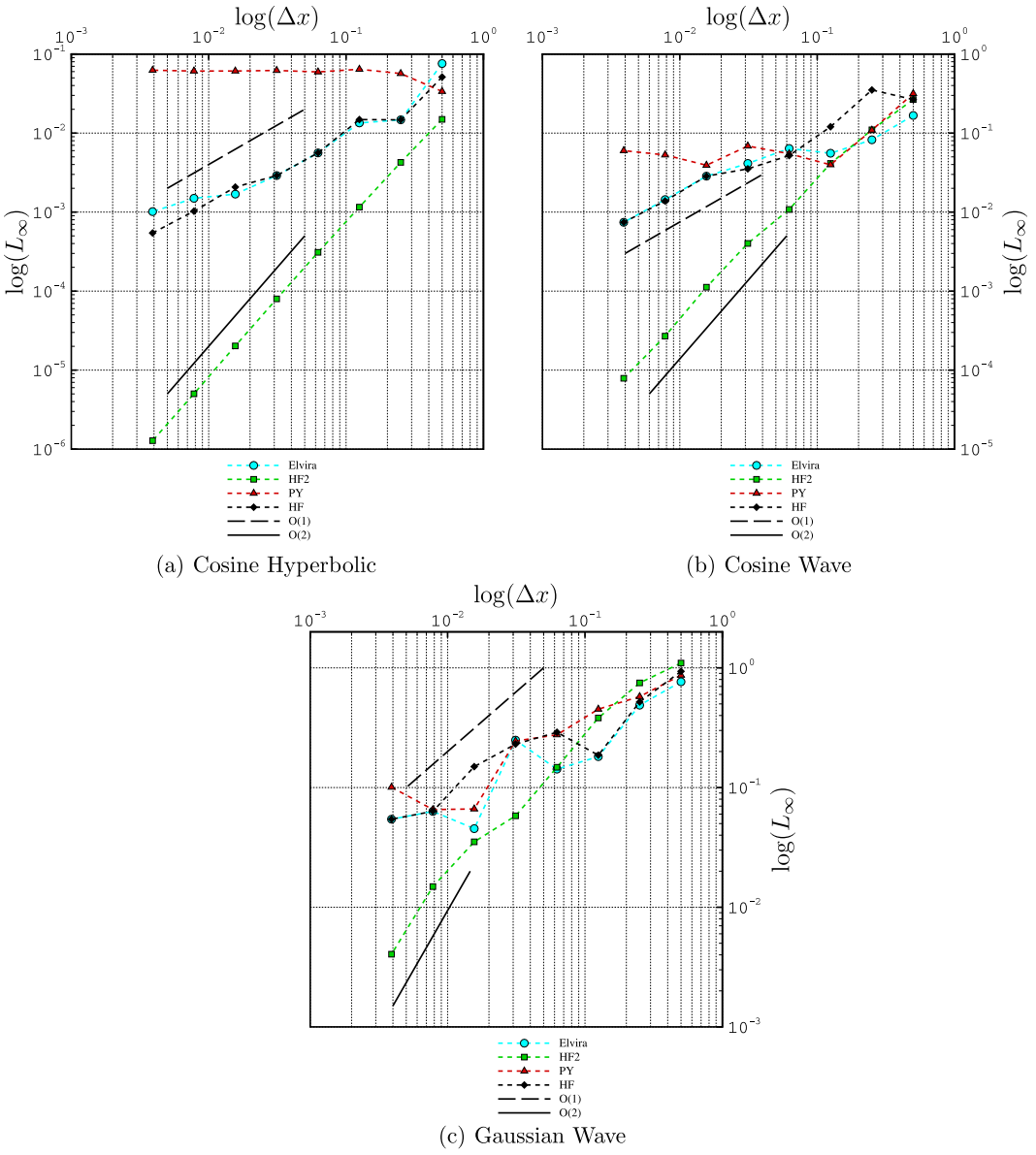

Fig. 7. Comparison of the L_∞ error norm for normals obtained by various methods.

are often applied to simulate complex phenomena involving dramatic interface deformation, when interfaces (or parts thereof) will be inevitably underresolved.

The L_∞ error norms for the other curves are shown in Fig. 7(a)–(c). These figures also show that HF2 yields the most accurate normal among all methods, especially when the mesh is refined and the interface is well-resolved. A bit more complicated than a circle, the cosine hyperbolic function (Eq. (17b) and Fig. 7(a)) features curvature and normal direction (the angle measured counterclockwise from a horizontal axis passing an arbitrary point on the curve) that vary slightly but monotonically between $[\frac{1}{5}\sqrt{\frac{1}{5}}, \frac{1}{5}\sqrt{\frac{3}{5}}]$ and $[-\tan^{-1}\sqrt{8}, -\tan^{-1}\sqrt{3}]$, respectively. Due to the small curvature that prevails over the domain, the interface is well-resolved everywhere. Except for the PY method, the smaller the curvature, the more accurate the normal.

The cosine wave (Eq. (17c) and Fig. 7(b)) is another step more complicated than the cosine hyperbolic function; the curvature varies between $[0, \pi^2/2]$ and the normal direction changes periodically. Again, HF2 maintains second-order accuracy with refinement, while the others do not.

Finally, we consider a Gaussian wave (Eq. (17d) and Fig. 7(c)). Here, curvature and normal direction vary abruptly and dramatically, and so the interface is not well-resolved everywhere. The maximum error occurs at $x = 1$ where the curvature is a maximum ($\kappa = 7.5$). Although the errors in this case are larger for all methods, HF2 is still one order of accuracy more

precise than the others. Also, Fig. 7(c) clearly indicates that on a coarse grid (less than 16×16), all methods behave similarly. But with refinement, HF2 reveals its second-order behavior, while other methods converge more slowly or not at all.

6. Conclusion

We have introduced an improved 2D height function (HF2) technique for calculating interface normals from volume fractions on structured meshes. A new definition for an "exact" averaged normal and for an error norm for normals have also been proposed, to compare the accuracy of different methods; this norm complements the well-known $\mathcal{L}^1$ norm that evaluates the position of a reconstructed interface relative to an exact one. The HF2 method is shown to be second-order accurate when evaluating both interface position and the normal. Finally, since the method relies solely on the known volume fractions and mesh geometry, we envision an extension of the methodology to 3D.

References

[1] D.J. Benson, Volume of fluid interface reconstruction methods for multi-material problems, Appl. Mech. Rev. 55 (2002) 151–165.
[2] J.U. Brackbill, D.B. Kothe, C. Zemach, A continuum method for modeling surface tension, J. Comput. Phys. 100 (1992) 335–354.
[3] S.J. Cummins, M.M. Francois, D.B. Kothe, Estimating curvature from volume fractions, Comput. Struct. 83 (2005) 425–434.
[4] M.M. Francois, S.J. Cummins, E.D. Dendy, D.B. Kothe, J.M. Sicilian, M.W. Williams, A balanced-force algorithm for continuous and sharp interfacial surface tension models within a volume tracking framework, J. Comput. Phys. 213 (2006) 141–173.
[5] D. Gueyffier, A. Nadim, J. Li, R. Scardovelli, S. Zaleski, Volume of fluid interface tracking with smoothed surface stress methods for three-dimensional flows, J. Comput. Phys. 152 (1999) 423–456.
[6] D.J.E. Harvie, M.R. Davidson, M. Rudman, An analysis of parasitic current generation in volume of fluid simulations, Appl. Math. Model. 30 (2006) 1056–1066.
[7] J. Helmsen, P. Colella, Non-convex profile evolution in two dimensions using volume of fluids, Lawrence Livermore National Laboratory, UCRL-ID-126402, 1997.
[8] C.W. Hirt, B.D. Nichols, Volume of fluid (VOF) methods for the dynamics of free boundaries, J. Comput. Phys. 39 (1981) 201–225.
[9] M. Malik, E.S.-C. Fan, M. Bussmann, Adaptive VOF with curvature-based refinement, Int. J. Numer. Meth. Fluids 55 (2007) 693–712.
[10] B.D. Nichols, C.W. Hirt, R.S. Hotchkiss, SOLA-VOF: A solution algorithm for transient fluid flow with multiple free boundaries, Los Alamos Scientific Laboratory, LA-8355, 1980.
[11] B.J. Parker, D.L. Youngs, Two and three dimensional Eulerian simulation of fluid flow with material interfaces, UK Atomic Weapons Establishment, 01/92, 1992.
[12] J.E. Pilliod Jr., E.G. Puckett, Second-order volume-of-fluid algorithms for tracking material interfaces, J. Comput. Phys. 199 (2004) 465–502.
[13] W.J. Rider, D.B. Kothe, Reconstructing volume tracking, J. Comput. Phys. 141 (1998) 112–152.
[14] M. Rudman, Volume-tracking methods for interfacial flow calculations, Int. J. Numer. Meth. Fluids 24 (1997) 671–691.
[15] R. Scardovelli, S. Zaleski, Direct numerical simulation of free-surface and interfacial flow, Annu. Rev. Fluid Mech. 31 (1999) 567–603.
[16] R. Scardovelli, S. Zaleski, Interface reconstruction with least-square fit and split Eulerian–Lagrangian advection, Int. J. Numer. Meth. Fluids 41 (2003) 251–274.
[17] D.L. Youngs, Time-dependent multi-material flow with large fluid distortion, in: K.W. Morton, M.J. Baines (Eds.), Numerical Methods for Fluid Dynamics, Academic Press, 1982, pp. 273–285.